Journal of Biomedical Optics

SPIEDigitalLibrary.org/jbo

In vivo spectral imaging of different cell types in the small intestine by two-photon excited autofluorescence

Regina Orzekowsky-Schroeder
Antje Klinger
Björn Martensen
Maike Blessenohl
Andreas Gebert
Alfred Vogel
Gereon Hüttmann

In vivo spectral imaging of different cell types in the small intestine by two-photon excited autofluorescence

Regina Orzekowsky-Schroeder,[a] Antje Klinger,[b] Björn Martensen,[a] Maike Blessenohl,[b] Andreas Gebert,[b,*] Alfred Vogel,[a] and Gereon Hüttmann[a]
[a]University of Lübeck, Institute of Biomedical Optics, Peter-Monnik-Weg 4, Lübeck 23562, Schleswig-Holstein Germany
[b]University of Lübeck, Institute of Anatomy, Ratzeburger Allee 160, 23568 Lübeck, Germany

Abstract. Spectrally resolved two-photon excited autofluorescence imaging is used to distinguish different cell types and functional areas during dynamic processes in the living gut. Excitation and emission spectra of mucosal tissue and tissue components are correlated to spectra of endogenous chromophores. We show that selective excitation with only two different wavelengths within the tuning range of a Ti:sapphire femtosecond laser system yields excellent discrimination between enterocytes, antigen presenting cells and lysosomes based on the excitation and emission properties of their autofluorescence. The method is employed for time-lapse microscopy over up to 8 h. Changes of the spectral signature with the onset of photodamage are demonstrated, and their origin is discussed. [DOI: 10.1117/1.3655587]

Keywords: two-photon microscopy; autofluorescence; small intestine; hyperfluorescence.

Paper 11001RR received Jan. 2, 2011; revised manuscript received Oct. 1, 2011; accepted for publication Oct. 4, 2011; published online Nov. 15, 2011.

1 Introduction

With its enormous surface area (~400 m^2 in humans), the intestine constitutes the most prominent boundary between the body and the environment. The intestinal wall serves, on the one hand, as a barrier between exterior and interior milieus. On the other hand, it ensures resorption and directed transport of nutrients from the outside, the lumen, into the organism. Both elementary functions are mainly fulfilled by the epithelium of the intestinal mucosa that completely lines this hollow organ. The majority of the epithelial cell monolayer is made of enterocytes with a predominantly resorptive function. However, numerous cells of the immune system constantly reside and move within the epithelium and the underlying tissue layer,[1] the so-called lamina propria, to prevent invasive or toxic pathogens and other alien substances from entering the organism. Furthermore, organized lymphoid tissue is found near all mucosae; in the case of the small intestine, in the Peyer's patches. Here, specialized epithelial cells, named M cells, take up antigens from the lumen.[2] Contact of immune cells, such as lymphocytes, and antigen presenting cells with relevant antigens below the M cells and possibly also below enterocytes of intestinal villi can then trigger a specific immune response.[3,4] In order to gain insight into the dynamics of this highly complex system, an *in vivo* time-lapse and three-dimensional imaging modality with subcellular resolution is needed that allows for reliable and nondamaging discrimination of the various cell types.

Two-photon excited fluorescence microscopy meets these requirements. It was established as a valuable tool in biology and life sciences soon after its first demonstration by Denk et al. in 1990.[5] In this technique, fluorescent molecules are excited via simultaneous absorption of two near-infrared photons that can deeply penetrate into the tissue. The high spatial and temporal photon density needed for this nonlinear process is achieved using tightly focused femtosecond laser pulses. The excitation laser beam is scanned over the sample, and the fluorescent light is collected at each scanning position with a photomultiplier tube. For spectral imaging, the fluorescent light is split by a grating, a prism, or dichroic mirrors into different wavelength channels that are detected by a line detector or separate photomultiplier tubes. The total detected time-averaged fluorescence intensity $\langle F(t)\rangle$ of each pixel depends on time-averaged laser power $\langle P(t)\rangle$ and laser pulse duration τ at the sample and is directly proportional to the two-photon absorption cross sections σ_{2P}, the concentration C, and the fluorescence quantum yield η of the fluorophores as well as to the detection quantum efficiency ϕ of the system. For a single chromophore, this is[6]

$$\langle F(t)\rangle \propto \phi\eta\sigma_{2P}C\frac{\langle P(r,t)\rangle^2}{\lambda\tau}, \quad (1)$$

where λ is the excitation wavelength. The product of the chromophore's fluorescence quantum yield η and its two-photon absorption cross section σ_{2P} is called two-photon action cross section σ'_{2P} and is experimentally more accessible than the pure two-photon absorption cross section.

From repeated scans of a stack of images of adjacent focal planes, time-lapse volume images can be generated. Compared to confocal laser scanning microscopy, which can also generate time-lapse and three-dimensional data with high resolution, two-photon microscopy has two main advantages. First, because infrared photons are used to excite the fluorophores, penetration

*Currently at: Friedrich-Schiller-Universität Jena, Institute of Anatomy II, Teichgraben 7, Jena 07740, Germany.

Address all correspondence to: Gereon Hüttmann, University of Lübeck, Institute of Biomedical Optics, Peter-Monnik-Weg 4, 23562 Lübeck, Germany; Tel: 0049-451-500-6530; Fax: 0049-451-500-6546; E-mail: huettmann@bmo.uni-luebeck.de.

1083-3668/2011/16(11)/116025/13/$25.00 © 2011 SPIE

depths of more than $>100\ \mu$m can be reached even in strongly scattering tissues.[7] In conventional fluorescence microscopy, the chromophores are mostly excited using UV/blue wavelengths that are strongly scattered in biological tissue, which limits the optical penetration depth to a few tens of micrometers. Second, the nonlinear absorption process leads to an intrinsic depth selection, because only in the focal region is the photon flux density high enough to excite fluorescence. Hence, no additional pinhole is needed in the detection path of the microscope and, most notably, photodamage and photobleaching are confined to the focal region as well. Minimization of photodamage is essential, especially for long-time *in vivo* studies of dynamic processes in which the biological system should be perturbed as little as possible.

In recent years, cell dynamics in a variety of complex living tissues have been studied using two-photon microscopy with exogenous markers and/or fluorescent proteins. These include skin,[8] kidney,[9] and lymphatic tissue.[10] Konjufca and Miller have reviewed the potential of two-photon microscopy as a tool to study the dynamics of host-pathogen interactions *in vivo*.[11] In the intestine, two-photon microscopy with a molecular marker has been used to study the epithelial barrier function *in vivo*,[12] to shed light on the role of dendritic cell extension into the lumen for pathogen sampling and uptake,[13] and to demonstrate goblet cell imaging as a marker for intestinal metaplasia of the stomach.[14]

Autofluorescence from many endogenous chromophores can be excited by a two-photon process within the tuning range of a Ti:sapphire laser.[15] Additionally, the collagen framework of the extracellular matrix yields a second-harmonic generation (SHG) signal of the focused femtosecond laser pulse at half the wavelength.[16,17] It has been demonstrated that, based on autofluorescence contrast, microscopic imaging of highly dymnamic tissues is possible *in vivo*.[18] This opens the possibility to use molecular markers for specific questions that are not related to general tissue morphology. Even more importantly, experimental complexity is reduced and the use of intrinsic fluorescence is expected to be less invasive to the organism than the use of molecular markers, which are usually phototoxic.[19] Furthermore, because there are only a few FDA-approved fluorescence contrast agents, the use of autofluorescence is most promising for any future clinical application.

Spectral information about cellular autofluorescence complements the morphological aspect of two-photon microscopy and can be used to delineate different structures in images of thick tissues with a submicron resolution without additional staining[20] or give a metabolic picture of the sample.[21,22] Ti:sapphire femtosecond lasers allow the excitation wavelength to be tuned in the range of 700–1000 nm and thus enable one to use differences in the excitation spectra for discrimination of fluorescent components. Furthermore, the fluorescence emission can be spectrally analyzed. By combining excitation and emission spectroscopy, two-dimensional spectral fingerprints of tissues and cells can be acquired.[23,24]

In vivo autofluorescence excitation-emission fingerprinting with a limited number of spectral channels has been demonstrated for the relatively static and easily accessible tissue of skin,[23] while cellular dynamics has been studied, autofluorescence based, only without the additional benefit of spectral information.[18] It is still a challenge to apply spectrally resolved two-photon autofluorescence imaging to dynamic structures, such as moving immune cells in the intestine under normal physiological conditions, because endogenous chromophores have a low two-photon absorption cross section,[15,25] resulting in a low signal. Furthermore, the maximum applicable excitation power that would improve imaging speed and image quality is limited by photodamage.

In this work, we show that two-photon excited autofluorescence allows imaging of the intestine *in vivo* with good contrast and subcellular resolution. *In vivo* excitation and emission measurements of two-photon excited cellular autofluorescence spectra are presented for cells and cell organelles in murine small intestine and are linked to spectra of endogenous chromophores. The possibility of generating multiparameter spectral fingerprints of different cell types is demonstrated. We show that selective fluorescence excitation with two separate wavelengths is beneficial for discrimination of epithelial enterocytes and antigen presenting cells. This information lays the basis for future automated identication of cells in images of this highly dynamic tissue or as a tool for targeted manipulation of single cells based on their spectral autofluorescence characteristics. Time-lapse imaging over up to 8 h while maintaining physiological conditions in healthy intestinal tissue is demonstrated. Photodamage reveals itself in a drastic increase of the emission intensity and a change of spectral characteristics, which may be used for online dosimetry of safe imaging.

2 Materials and Methods

2.1 *Mouse Model*

In vivo experiments were carried out using female anaesthetized balb/c mice. First, a tracheostomy was performed, and the mouse was connected to a ventilator (Hugo Sachs Elektronik - Harvard Apparatus GmbH, March-Hugstetten, Germany) [Fig. 1(a)]. Then, the abdominal cavity was opened and a loop of the small intestine was surgically prepared *in situ* [Fig. 1(b)]. The loop was fixed using Vetbond glue (3M, St. Paul, Minnesota) onto a heated block with an electronic temperature control and opened lengthwise in order to access the mucosa. The tissue was flushed with 37 °C ringer solution several times to remove intestinal contents. During imaging, the mucosa was slightly pressed against a fixed microscope coverslip [Figs. 1(b) and 1(c)]. This procedure minimized movement artifacts due to peristalsis. The mouse holder was tempered to 37 °C, and the subject's vital parameters were monitored with a pulse oximeter at the tail vein (MouseOx, Starr Life Sciences, Oakmont, Pennsylvania) [Fig. 1(a)]. To prevent heat drain through the microscope objective, it was equipped with objective heating [Fig. 1(a)].

2.2 *Spectral Imaging by Two-Photon Excited Autofluorescence*

Autofluorescence imaging was done with a modified JenLab DermaInspect two-photon microscope (JenLab GmbH, Jena, Germany). Figure 2(a) shows schematics of the setup. The fluorescence excitation source was a femtosecond Ti:sapphire laser tunable between 710 and 920 nm, with a pulse repetition rate of 80 MHz (MaiTai, Newport Spectra-Physics, Irvine, California). A Zeiss 40x/1.2 w C-Apochromat objective was used to focus

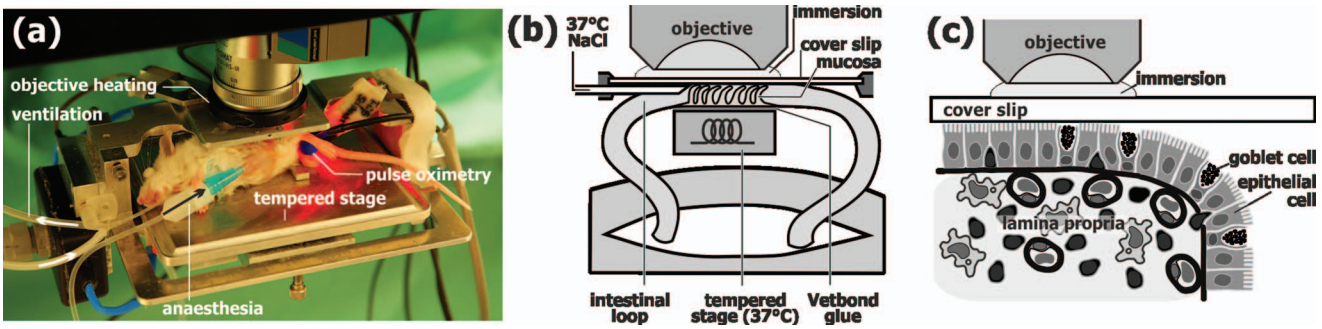

Fig. 1 Setup for the investigation of murine intestinal mucosa *in vivo*. (a) Anaesthetized balb/c mouse on a homeothermic table. Respiration and oxygen saturation were monitored by pulse oximetry. Physiological temperature (37 °C) was maintained by feedback-controlled heating of stage and objective. During surgical preparation, the abdominal cavity of the anaesthetized mouse was opened and an isolated intestinal loop was prepared *in situ* without disturbing the blood supply as shown in (b). The intestine was glued onto a tempered sample stage and sliced lengthwise, so that the mucosa could be carefully pressed to a fixed coverslip. The enlarged view in (c) shows a schematic diagram of the intestinal mucosa (not true to scale).

the excitation light onto the sample and collect the fluorescence light (Carl Zeiss Jena GmbH, Jena, Germany). The field of view of 150 × 150 μm^2 was sampled with 512 × 512 pixels.

For spectral imaging, we inserted a four-channel spectral detector into the fluorescence path consisting of four photomultiplier tubes (Hamamatsu R1294A and R1295A, Hamamatsu Photonics Deutschland GmbH, Herrsching am Ammersee, Germany) and a set of dichroic filters. The dichroic filters were chosen to provide a good separation between known fluorescence emission spectra of endogenous fluorophores. Of particular interest is a separation of the reduced forms of nicotinamide adenine dinucleotides [NAD(P)H] from other chromophores. NAD(P)H is crucial for cell metabolism and is found in high concentrations at the mitochondria.[26] Enterocytes are metabolically very active and thus contain a large number of mitochondria for the synthesis of adenosine tri-phosphate. In order to spectrally characterize the four detection channels, transmission measurements of all optical elements except for the objective were performed. Transmission data of the manufacturer were used for the microscope objective. Figure 2(b) shows the spectral characteristics of our fluorescence detection system, including detector quantum efficiency (solid lines, right scale) in comparison to emission spectra of endogenous fluorophores as reported in Refs. 27 and 28 (symbols, left scale).

From the intensity images recorded in the four spectral channels, false-color images were produced. The colors were chosen as follows: blue for channel 1, $\lambda \approx 380$–450 nm; green for channel 2, $\lambda \approx 450$–500 nm; red for channel 3, $\lambda \approx 500$–580 nm; and pink for channel 4, $\lambda \approx 580$–680 nm (Fig. 3).

To obtain excitation spectra, subsequent images of the same structure were recorded while the two-photon excitation wavelength was varied between 730 and 910 nm. For each excitation wavelength, the average laser power at the sample was adjusted such that autofluorescence signal of all relevant biological structures was above the noise level, while staying below the threshold for photodamage. Acquisition times of 7.4 or 13.4 s were required to record single images.

2.3 *Image Analysis*

In order to spectrally distinguish different cells and cell organelles, we were interested in the material-specific fluorescence intensity characteristics as a function of excitation and emission wavelength. As is evident from Eq. (1), for an excitation wavelength λ_{ex}, the total recorded fluorescence intensity of a single chromophore is directly proportional to the product of two-photon action cross section $\sigma'_{2P}(\lambda_{ex})$ and the concentration

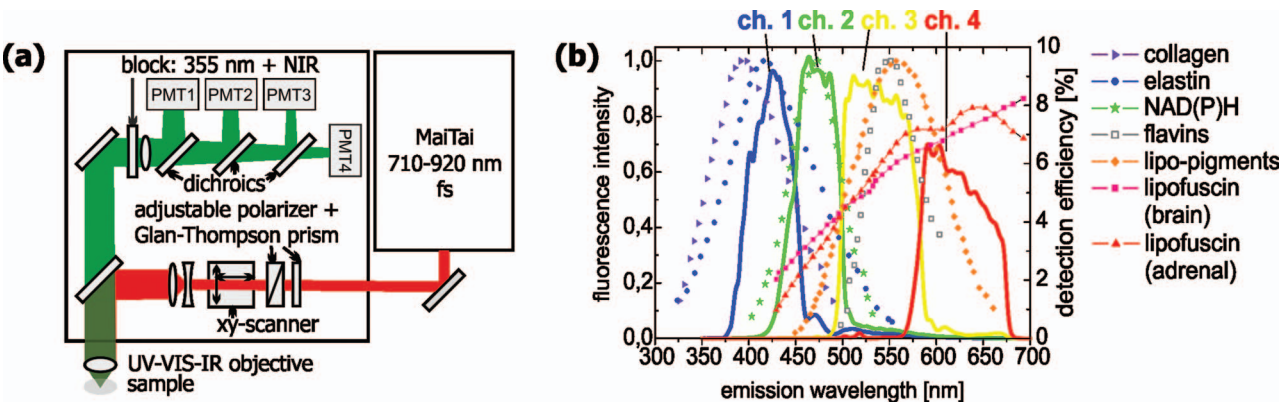

Fig. 2 Spectral imaging. (a) Schematic drawing of the two-photon microscope with fluorescence emission detection in four spectral channels. (b) Spectral detection probability of the four detection channels, including the transmission of all optical elements and the quantum efficiency of the photomultipliers (solid lines, right axis). For comparison, emission spectra of important endogenous chromophores as reported in Refs. 27 and 28 are also shown (symbols, left axis). NAD(P)H: nicotinamide adenine dinucleotide and nicotinamide andenine dinucleotide phosphate.

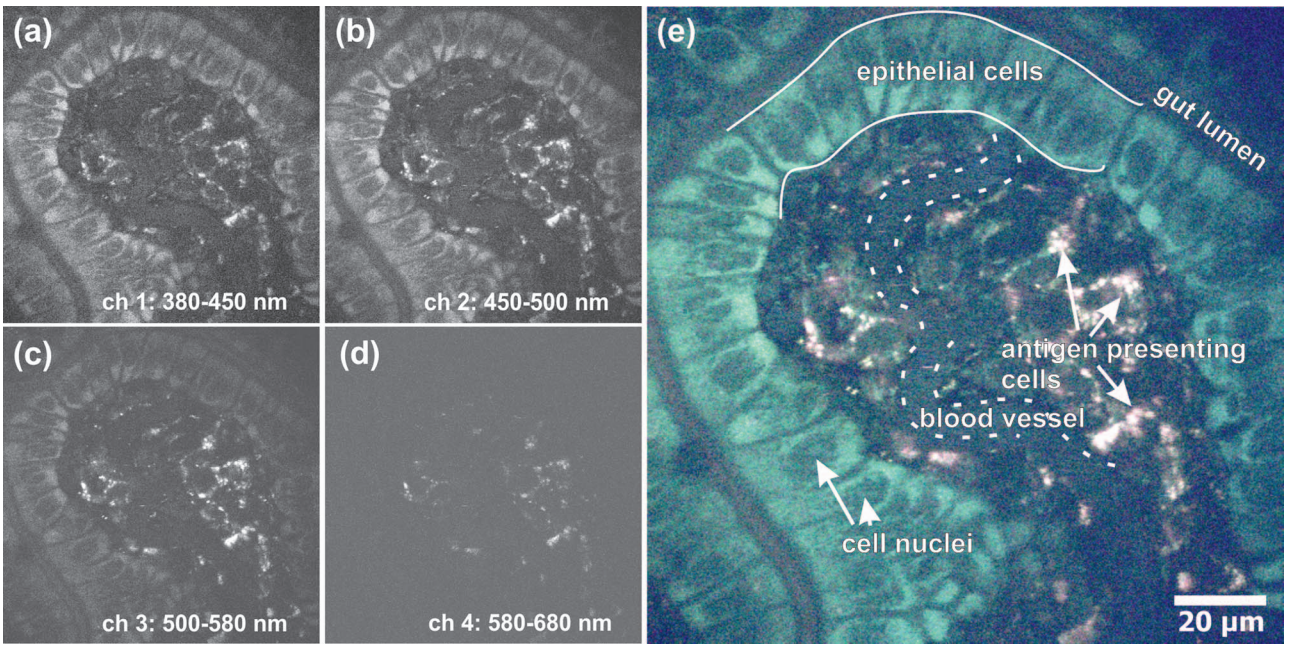

Fig. 3 Crosssectional autofluorescence image of intestinal villus *in vivo* measured in four spectral channels. (a–d) Intensity images of each channel. (e) False color overlay with marked structures of interest. Excitation wavelength $\lambda_{ex} = 750$ nm, image size 512 × 512 pixel.

C of the chromophore in the sample. This product is specific for each sample. All other factors in the equation are inherent to the imaging system and apply equally to all samples.

In cells, a mixture of different chromophores is expected to contribute to the fluorescence intensity in each pixel. Following Eq. (1), the sum of these contributions can be described as

$$\langle F(t)\rangle \propto \frac{\langle P(r,t)\rangle^2}{\lambda_{ex}\tau} \sum_i \sigma'_{2P_i}(\lambda_{ex}) C_i . \tag{2}$$

Laser excitation power and pulse duration vary with excitation wavelength. In order to calculate the cell-specific or cell organelle–specific fluorescence intensity as a function of excitation wavelength, we thus needed to correct the measured fluorescence intensity for the mean power $\langle P\rangle$ at the sample and the laser pulse duration τ and excitation wavelength λ_{ex}

$$\langle F(t)_{corr}\rangle = \langle F(t)\rangle \frac{\lambda_{ex}\tau}{\langle P(r,t)\rangle^2} \propto \sum_i \sigma'_{2P_i}(\lambda_{ex}) C_i . \tag{3}$$

The laser pulse duration was measured by means of an autocorrelator (PulseCheck, APE GmbH, Berlin, Germany) at a location where the pulses were transmitted through the microscope but had not yet entered the objective. The pulse duration was obtained by fitting the autocorrelation function to a sech^2-function. For wavelengths of >880 nm, the laser intensity was too small for measuring the laser pulse duration. Therefore, only data up to this wavelength were used for evaluation of the fluorescence emission spectra. Measurement of the emission spectra of the laser confirmed that the pulses were Fourier-transform limited. To account for pulse broadening in the two-photon microscope, we determined the group delay dispersion of the DermaInspect and the objective, separately, and calculated the pulse length after transmission through the entire microscope.

The mean laser power at the sample was measured after each experiment using an integrating sphere (model no. 69, Delta Developments, Liss, Hants, United Kingdom). Because direct measurements with the water immersion objective were not possible, we measured the power entering the back entrance pupil of the objective. This was achieved by using an aperture stop of the same size as the back aperture of the objective and measuring the power behind this aperture. Data were then corrected for the objective's transmittance as provided by the manufacturer.

For generating excitation and emission spectra of specific cells and cellular structures, regions of interest (ROIs) were defined in the images. The ROIs were selected manually according to tissue morphology and delineated using the image-analysis software[29] ImageJ. ROIs were the apical cytoplasm of enterocytes (ECs), bright punctuate regions, presumably lysosomes, within the apical cytoplasm of enterocytes, and antigen-presenting cells (APCs) that contained many bright granules in the lamina propria of villi and Peyer's patches. For each excitation wavelength, 4–20 ROIs of the same type were evaluated in an image and the average intensity value and standard error of the mean of these ROIs were calculated for each emission channel. A channel-specific mean background value as recorded in a dark measurement without laser irradiation was subtracted from this value. Subsequently, data were corrected for the experimental parameters according to Eq. (3).

The corrected average fluorescence intensity $\langle F_{corr}\rangle$ as a function of excitation wavelength was analyzed in order to characterize enterocytes and antigen-presenting cells within the lamina propria of Peyer's patches and villi by their spectral excitation-emission fingerprints. The specific excitation spectrum of the respective cell type or tissue structure was calculated for each ROI type by integrating the mean fluorescence intensity over all four emission channels for each excitation wavelength λ_{ex}. Excitation-emission spectra were produced by plotting $\langle F_{corr}\rangle$

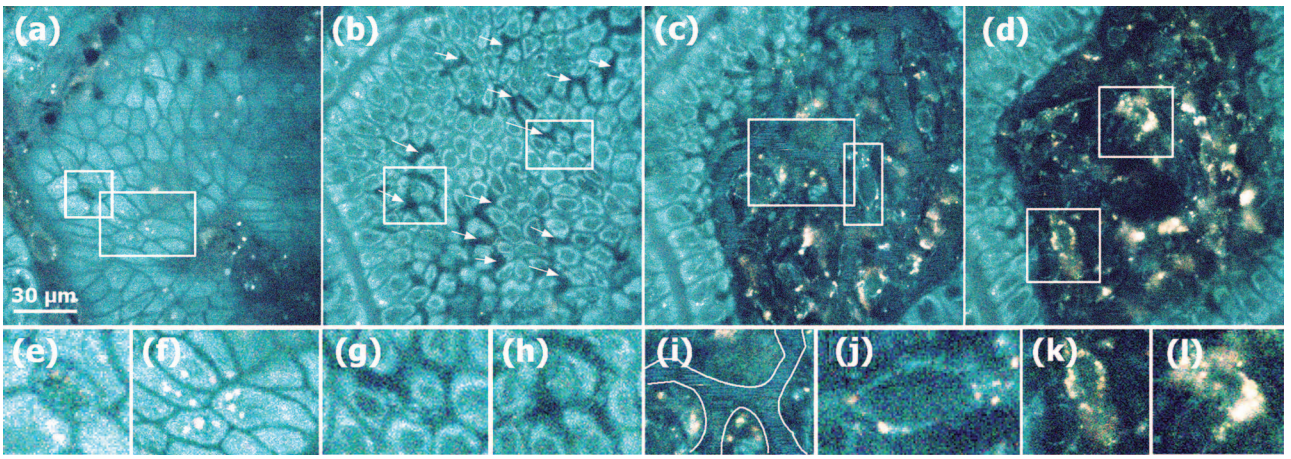

Fig. 4 (Video 1) Image stack through a 33-μm depth of an intestinal villus. Excitation wavelength $\lambda_{ex} = 730$ nm, image size 150×150 μm^2. (a) 1.6-μm depth. Goblet cells appear dark in the bright mosaic pattern of enterocytes. (b) 13.6-μm depth. Black intraepithelial lymphocytes reside between the basal part of the prismatic epithelial cells. Cell nuclei appear dark. (c,d) 22.4- and 25-μm depth. Antigen-presenting cells filled with bright granules, fibroblasts, and blood vessels are visible in the lamina propria. Details of the image stack: (e) goblet cell, (f) epithelial lysosomes, (g,h) intraepithelial lymphocytes, (i) capillary vessel, (j) fibroblast, and (k,l) antigen presenting cells. (Quick Time, 2.5 MB). [URL: http://dx.doi.org/10.1117/1.3655587.1]

for each emission channel as a function of excitation wavelength. From these data, emission spectra at two fixed excitation wavelengths were calculated.

3 Results and Discussion

3.1 *Spectrally Resolved Images of Cell Motility in the Small Intestine Based on Intrinsic Contrast*

Using spectrally resolved two-photon excited autofluorescence microscopy, we imaged and identified different cell types of the small intestinal mucosa *in vivo*. Figure 3 shows an autofluorescence image of an optical cross section through an intestinal villus 25 μm below the tissue surface taken with a 750-nm excitation wavelength. The villus is lined by columnar, prismatic epithelial cells that exhibit a strong fluorescence signal from the cytosol and mitochondria (blue-green in the false-color image), while the cell nuclei appear dark. The epithelium is clearly delineated from the underlying lamina propria, a loose connective tissue that contains various cell types of different morphology, such as antigen-presenting cells, lymphocytes, and fibroblasts (see also Figs. 4–6). Antigen-presenting cells contain many lysosomes, which appear as bright reddish or white granules in the false-color image. Capillaries of the blood vascular system can also be identified. Erythrocytes emit a weak autofluorescence signal and, because they are moving fast during image acquisition, appear as faint lines parallel to the scanning direction of the laser beam in the fluorescence image (see Fig. 4 and Video 1). Observation of these movement traces during the experiments served as additional and instantaneous indication that physiological conditions were maintained, because movement traces are not visible when blood circulation of the tissue is compromised.

By recording stacks of optical sections at different depth, we can resolve the three-dimensional morphology of small intestinal mucosa *in vivo*. Fig. 4 (Video 1) shows an image stack of a volume 150×150 μm^2 covering a 33-μm depth starting in the lumen just above the tip of an intestinal villus. At a 1.6-μm depth, the epithelium appears as a mosaic of bright areas with dark borders [Fig. 4(a)]. In contrast to the bright cytosol of enterocytes, the outline of the cells appears dark. Dark areas in the mosaic were identified as mucus-containing goblet cells. The mucus itself does not fluoresce, but cytosol and mitochondria below the mucus granules do show fluorescence [Fig. 4(e)]. In some enterocytes, bright reddish granules appear in the apical cytoplasm [Fig. 4(f)]. These granules are most likely lysosomes, which are known to be located predominantly in the apical cytoplasm of enterocytes. Cell nuclei of enterocytes start to appear at ~4 μm depth and extend up to 16 μm depth [Fig. 4(b)]. The nuclei appear dark in the autofluorescence image because they contain only low concentrations of NADH.[30] At ~14 μm depth, dark cells are found between the enterocytes [Figs. 4(b), 4(g), and 4(h)]. These are intraepithelial lymphocytes in which the nonfluorescent cell nucleus makes up most of the cell volume. These lymphocytes reside only in the basal part of the epithelium, right above the basement membrane. The basement membrane itself is located at ~17.5 μm depth in this image stack and is not visible in the autofluorescence image. Below the basement membrane, capillaries, fibroblasts, and antigen-presenting cells can be seen in the lamina propria of the villus [Figs. 4(i)–4(l), respectively]. Antige- presenting cells contain many reddish lysosomes [Figs. 4(c), 4(d), 4(k), and 9(l)]. From a 26-μm depth on, a dark area devoid of cells appears in the middle of the lamina propria (Video 1). This is most likely a lymph vessel.

Another dimension of information about the biological system is added, when the same field of view is imaged repeatedly over time. Fig. 5 (Video 2) shows a cross section of an intestinal villus similar to Fig. 3. The field of view was recorded repeatedly every 40 s over a time period of 13 min. The time-lapse video reveals that the living intestinal mucosa is a highly dynamic system. Cells in the lamina propria of a villus move, interact, and change shape. Intraepithelial lymphocytes in the basal part of the epithelium are also constantly in motion. A detailed analysis of these cellular dynamics will be published elsewhere.

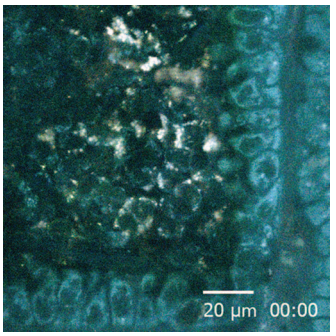

Fig. 5 (Video 2) Time series of a cross-sectional view of an intestinal villus covering 13 min. A frame was recorded every 40 s. Excitation wavelength $\lambda_{ex} = 730$ nm, image size 150×150 μm^2. Cells in the lamina propria as well as intraepithelial lymphocytes move and interact during the observation period. (Quick Time, 3.5 MB). [URL: http://dx.doi.org/10.1117/1.3655587.2]

Figure 6 shows a series of false-color, two-photon excited autofluorescence images of an intestinal villus taken at different excitation wavelengths. The cytoplasm of enterocytes fluoresces merely at shorter excitation wavelengths. At >800 nm, within enterocytes only the fluorescence of the bright granular cell organelles in the apical part of the cells is excited. The spectral emission of antigen-presenting cells and enterocytes show significant differences for excitation at shorter wavelengths: enterocytes appear blue-greenish with a dark nucleus whereas antigen-presenting cells are filled with reddish bright granules. In contrast, antigen-presenting cells in the lamina propria yield a strong signal up to the longest available excitation wavelengths. As the excitation wavelength becomes longer, the entire images appear more reddish. This is due to the fact that only fluorophores with lower excitation energies and, thus, a redder emission spectrum can be excited. Figure 7 shows an equivalent excitation wavelength series for the lamina propria of a Peyer's patch at the same magnification. There are more and finer bright granules within the cells compared to the villus lamina propria. Furthermore for $\lambda_{ex} \geq 790$ nm blue SHG signal is emitted from the collagen cross links of the extracellular matrix. The epithelium lies ~ 12 μm above the focal plane and is not visible in this image series.

3.2 *Autofluorescence Spectra of Cells and Cell Constituents in the Small Intestine*

Distinct cellular structures and cell populations can be associated with the two main functions of the small intestinal mucosa (i.e., digestion and barrier). To identify the relevant cells, we were interested in the autofluorescence spectra of the following tissue components: enterocytes and lysosomes within enterocytes as representatives for resorption, and antigen-presenting cells in two different functional areas, the villi and Peyer's patches, as representatives for pathogen sampling and uptake. Antigen presenting cells in the lamina propria of villi and the gut-associated organized lymphoid tissue, the Peyer's patches, have different functions and consist of different cell populations. Gastrointestinal macrophages are present mostly in the subepithelial lamina propria of villus in the small intestine[31] and believed to be crucial for tissue homeostasis. It has been proposed that antigens, resulting from digestion in the lumen and transepithelially transported or degraded intracellularly in enterocyte lysosomes could associate with MHC II and be presented to lymphocytes to suppress the systemic immune response to luminal antigens, such as digested food products.[32–34] In the subepithelial dome area of organized mucosal lymphoid tissue, the

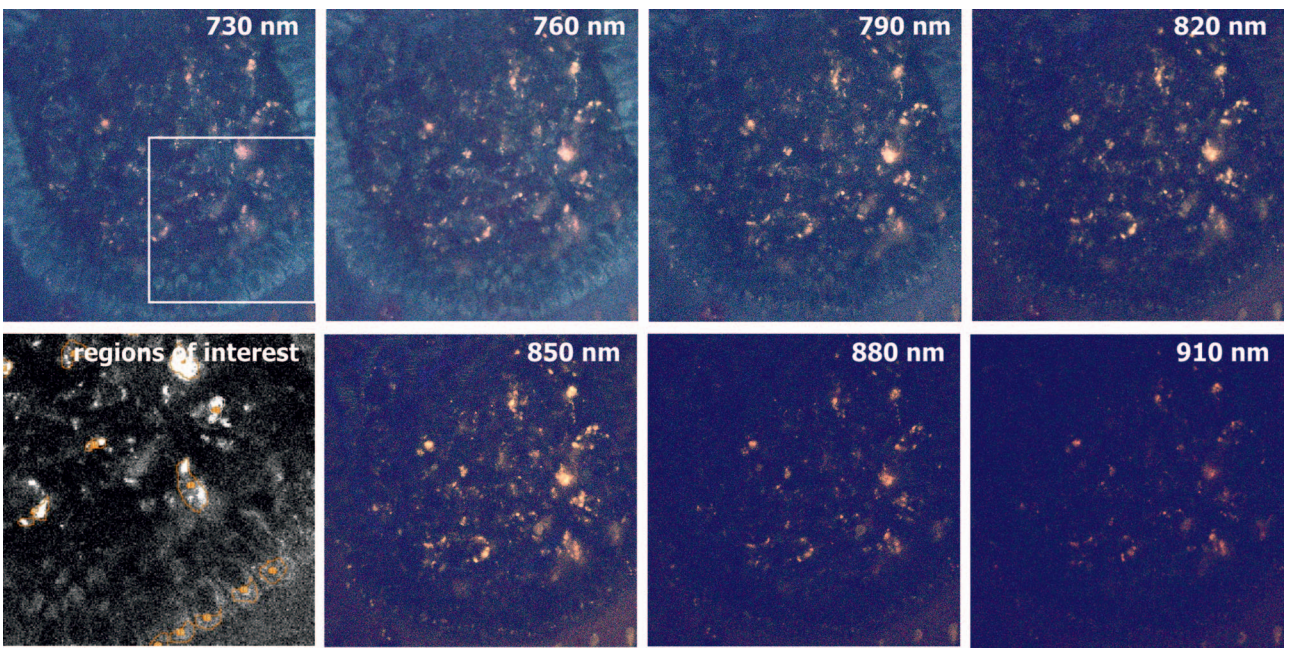

Fig. 6 Autofluorescence images of an intestinal villus taken at different two-photon excitation wavelengths. Images are false-color overlays of four-channel intensity images as described in Sec. 3. Enterocyte fluorescence is excited only up to 790 nm, while antigen-presenting cells in the lamina propria and epithelial lysosomes yield a strong fluorescence signal over the whole excitation spectrum. In the lower left image, selected regions of interest are exemplarily marked in a region corresponding to the box in the image at 730 nm.

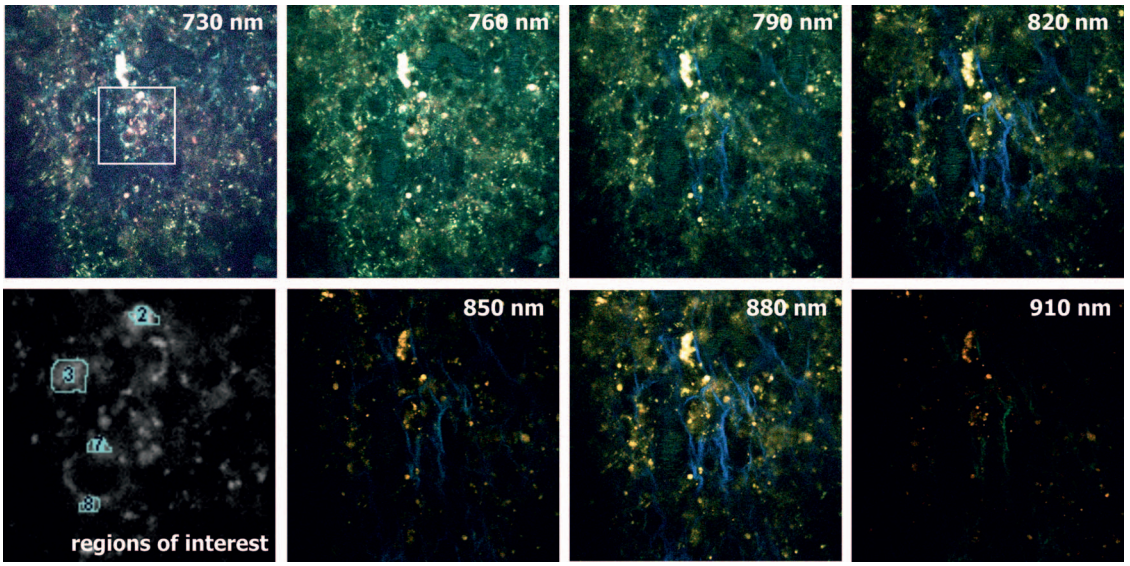

Fig. 7 Autofluorescence images of the lamina propria in a Peyer's patch taken at different two-photon excitation wavelengths. Images are false-color overlays of four-channel intensity images as described in Fig. 3. The morphology and inner structure of cells differs markedly from the villus lamina propria (Fig. 6). At excitation wavelengths ≥790 nm, (SHG) light is generated at the collagen framework of the extracellular matrix that is detected in the <450-nm emission channel and thus appears blue in the false-color images. In the lower left image, selected regions of interest are exemplarily marked in in a region corresponding to the box in the image at 730 nm.

Peyer's patches, the dominant antigen-presenting cells are dendritic cells,[35] which are desigend to process antigens and initiate specific immune response. In the follicle-associated epithelium, specialized epithelial M cells deliver samples of foreign material through active transpeithelial vesicular transport from the lumen directly to intraepithelial lymphoid cells.[36] Thus, it is conceivable that these different cell populations from diverse functional areas might contain different mixtures or concentrations of fluorescent molecules and thus show different spectra.

Figure 8(a) shows autofluorescence excitation spectra for the cytoplasm of enterocytes, antigen-presenting cells, and lysosomes within enterocytes. We observed variations in absolute fluorescence intensity for the same cell type between different λ stacks recorded in different experiments. These variations were caused by variations in tissue thickness, amount of mucus, remnants of luminal content, etc. Therefore, the excitation spectra in Fig. 8 were normalized to the intensity value at 730 nm to be able to compare data from different λ stacks. The fluorescence intensity in all enterocyte excitation spectra decreases by two orders of magnitude but maintained the same slope when increasing the excitation wavelength up to ~820 nm. For even longer wavelengths, the mean count rate of the autofluorescence signal from enterocytes lies within the standard deviation of the dark count rate. In contrast, antigen-presenting cells in villi and Peyer's patches show a weak decrease in fluorescence intensity with increasing wavelength. The signal drops at most about one order of magnitude and is well above noise level, even for the longest available excitation wavelengths. This corresponds to the good visibility of antigen-presenting cells over the whole wavelength range, as seen in Fig. 6. The variation among the signals of antigen-presenting cells is stronger than for enterocytes, which may be explained by the broad variety of cell shapes and inner structure (granulation). As cells move and change shape, the cell content within the ROIs may slightly vary from frame to frame during wavelength tuning, which may affect the extracted mean intensity values. However, cell parts entering and leaving the image plane should balance, on average, because a coordinated directed movement of antigen-presenting cells is not expected.

The bright punctuate cell organelles in the apical cytoplasm of enterocytes show a similar excitation spectrum to that of antigen-presenting cells [orange circles in Fig. 8(a)], which contain a large and dense amount of brightly fluorescent cell organelles. Several facts suggest that the bright punctuate organelles that are located within the apical cytoplasm of enterocytes and within antigen-presenting cells are most likely lysosomes. First, due to their function, antigen-presenting cells contain many lysosomes. Second, lysosomes are abundant in all cells that have a mainly resorptive function as have enterocytes. Third, from electron micrographic slides it is known that lysosomes in enterocytes are located preferably in the apical cytoplasm. This interpretation has been confirmed in an experiment using LysoTracker Red (Invitrogen). The red fluorescent dye stained the bright cell organelles in the apical cytoplasm of enterocytes within minutes when applied directly onto the intestinal mucosa.

Figure 9 shows excitation spectra obtained as above but now broken down into the spectral contributions from each emission channel. All spectra are taken from the same animal and were not normalized to be able to compare absolute intensity differences between different fluorescent structures. The emission spectra exhibit marked differences between the different tissue constituents. The cytoplasm of enterocytes in an intestinal villus [Fig. (9(c)] yields a significant signal only in the first three channels (i.e., the fluorescence emission spectrum lies below 580 nm). The emission >580 nm in the fourth channel is almost at background level. Therefore, the value is almost zero for 760 and 880 nm excitation and thus out of scale in Fig. 9(a). The signals in the first two channels (<500 nm) are about equal for

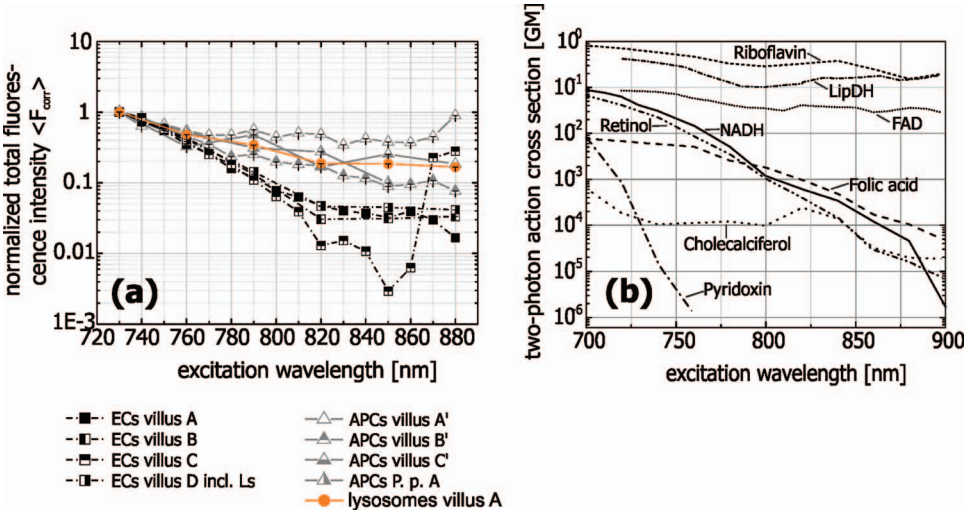

Fig. 8 (a) Measured excitation spectra of intestinal cells and cell organelles: ECs: cytoplasm of enterocytes, APCs: antigen presenting cells, Ls: lysosomes. Capital letters in the legend denote different experiments. For better comparison between different experiments, spectra are normalized to the intensity value at 730 nm. Spectra are further normalized to $P^2/(\lambda_{pulse})$ in order to correct for measured differences in experimental parameters. Here, P is the average laser power at the sample, λ the excitation wavelength, and τ pulse the pulse length at the sample. After normalization, the recorded intensity values are directly proportional to the two-photon absorption cross sections $\sigma_2 P$ of the excited chromophores. (b) Two-photon absorption cross sections for endogenous fluorophores as reported in Refs. 15 and 25.

an excitation wavelength up to 780 nm and brighter than the signal in the third channel (500–580 nm). The decrease of fluorescence intensity with increasing excitation wavelength is more pronounced for channels 1 and 2 than for channel 3. In all channels, excitation with wavelengths of >800 nm does not yield significant fluorescence emission from cytosol in enterocytes (see also Fig. 6).

The spectral autofluorescence emission of lysosomes in enterocytes of an intestinal villus is shown in Fig. 9(b). Fluorescence intensity is generally brighter, but the main difference as compared to the cytoplasm is a significant signal in the red emission channel that was negligible for the cytoplasm. Furthermore, the signal in the second channel (450–500 nm) is stronger than the short-wavelength contribution (<450 nm) detected in the first channel, and the fluorescence intensity decrease with increasing excitation wavelength is more pronounced for the first than for the second channel.

Antigen-presenting cells of the lamina propria of both villi [Fig. 9(c)] and Peyer's patches [Fig. 9(d)] show a strong emission of about equal intensity for all excitation wavelengths in the green and yellow channel. In contrast to enterocytes' cytoplasm and lysosomes, this signal is stronger than the fluorescence signal in the first channel for all excitation wavelengths. In the first channel, the signal decreases with increasing wavelength as for cytoplasm of enterocytes. Most likely, the cytoplasm of antigen-presenting cells has a composition similar to enterocytes' cytoplasm, which results in a component of similar autofluorescence spectrum. In addition, fluorescence emission in the red channel (>580 nm) is about a factor 10 stronger for antigen-presenting cells than for enterocytes at all excitation wavelengths. Compared to lysosomes, the signal in the red channel is stronger for antigen-presenting cells at short excitation wavelengths and decreases more rapidly with increasing excitation wavelength. Overall, the absolute intensities are distributed more equally between all four emisison channels (i.e., the emission spectrum of antigen-presenting cells is broader and shifted to the red as compared to cytoplasm and lysosomes of enterocytes).

The acquisition and comparison of complete excitation-emission spectra is very time consuming and not suited for a real-time discrimination of cells and cell organelles based on their autofluorescence spectra. However, ratiometric comparison of autofluorescence emission in the four emission channels or at two fixed excitation wavelengths could be used instead. Therefore, in Fig. 10 and Table 1 the spectral fluorescence emission of the different cells and cell organelles as shown in Fig. 9 is compared at 730 and 820 nm excitation.

In Table 1, we chose channel 2 as ratiometric reference channel following an approach taken by Huang et al.[25] They showed that, using 750 and 800 nm two-photon excitation and fluorescence emission channels of 410–490 and 510–650 nm, ratiometric imaging of NAD(P)H and flavoprotein in cardiomyocytes reflected the redox state of the cell. They also found that fluorescence excitation at 800 nm compensated for the large differences in the concentrations and two-photon absorption cross sections of NAD(P)H and flavin adenine dinucleotide (FAD) at the mitochondria and gave an almost balanced picture of the redox ratio. In our setup, NAD(P)H fluorescence is detected mainly in channel 2 (450–500 nm), while flavins fluoresce predominantly in channel 3 (500–580 nm). Consequently, the ratio of fluorescence intensities ch2/ch3 excited at 820 nm should best reflect the NAD(P)H/FAD ratio. At a 730-nm excitation, all four selected tissue components are visible and all of them peak at 450–500 nm emission. However, for the cytoplasm and lysosomes within enterocytes, the short-wavelength contribution from 380–450 nm is about as strong as the emission between 450 and 500 nm. This is reflected in a ratio close to 1 for ch2/ch1 in Table 1(a). The redshifted spectral emission of lysosomes as compared to the cytosol is represented by a lower ch2/ch3 ratio of lysosomes. The high ch2/ch4 ratio for cytoplasm of enterocytes has a large error and has to be disregarded

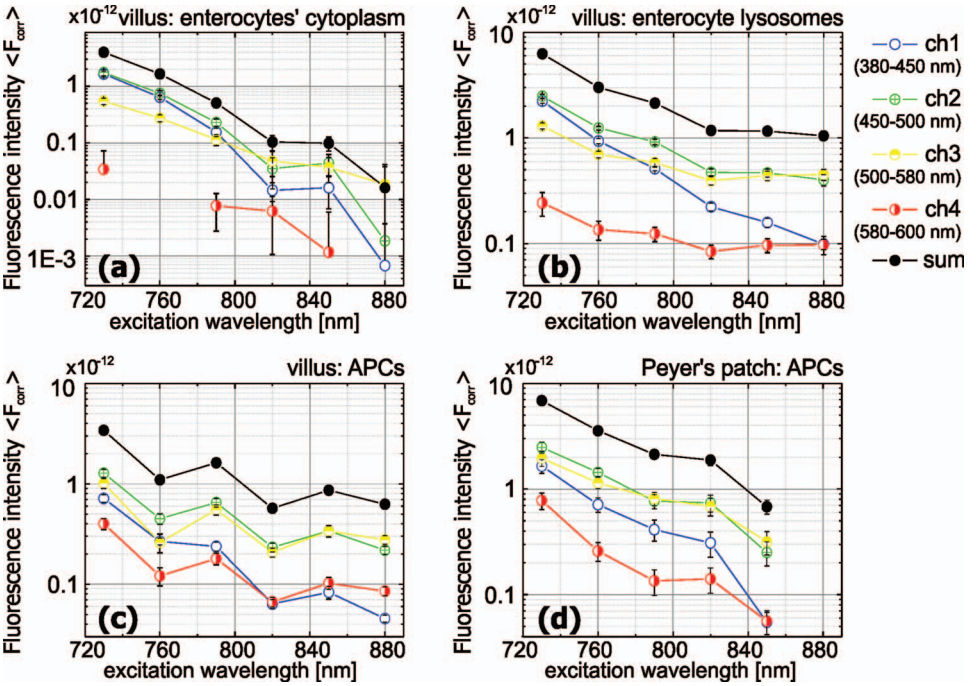

Fig. 9 Spectral excitation-emission characteristics of selected tissue components in the small intestine. (a) Apical cytoplasm of villus enterocytes ($n = 7$). (b) Villus epithelial lysosomes ($n = 15$). (c) Antigen-presenting cells (APCs) in the villus lamina propria ($n = 15$). (d) Antigen-presenting cells in the Peyer's patch (P. p.) lamina propria ($n = 11$). The average intensity from selected regions of interest is plotted on a semilogarithmic scale for each emission channel as function of excitation wavelength (open symbols). In addition, the sum intensity of all channels is shown (black dots). As in Fig. 8, intensity values are normalized to $P_2/(\lambda\tau_{pulse})$ in order to correct for measured differences in experimental parameters. All spectra are taken from the same animal in order to compare absolute differences in fluorescence intensity without normalization at 730-nm excitation. Error bars represent the standard error of the mean.

due to the marginal fluorescence intensity in channel 4. The ch2/ch3 ratios at 730- and 820-nm excitation show differences between enterocytes, lysosomes, and antigen-presenting cells. At 820 nm, this ratio is approximately the same for lysosomes and antigen-presenting cells, but lower for enterocytes. This difference must not necessarily be related to differences in the redox state of the cell populations but may originate from our ROI selection. While in enterocytes we selected regions in the apical cytoplasm containing a high amount of mitochondria, the ROIs in antigen-presenting cells comprise only a minor fraction of mitochondria and cytosol, but a large amount of the bright granules which we identified as lysosomes. Thus, although the ratio of emission intensities in ch2/ch3 discriminates between enterocytes and antigen-presenting cells, it does not necessarily tell about differences in the respective metabolic states. The ROIs selected for antigen-presenting cells in villi and Peyer's patches contain similar structures. Nevertheless, even though the cell populations and their tasks differ, the ch2/ch3 ratio does not show differences between these cell types within the error margins. If differences in the NAD(P)H/FAD ratio are present, they may not be observable because of the high lysosomal portion in the cells compared to the mitochondrial portion. The ch2/ch1 ratio is slightly larger for antigen-presenting cells in the lamina propria of villi than for antigen-presenting cells in the Peyer's patches. This indicates that antigen-presenting cells in villi contain fluorophores that emit in the short-wavelength range of ch1 in lower concentration or with lower two-photon absorption cross section than those in Peyer's patches. Table 1(c) indicates that antigen-presenting cells in Peyer's patches and villi can be even better distinguished when looking not only at a single

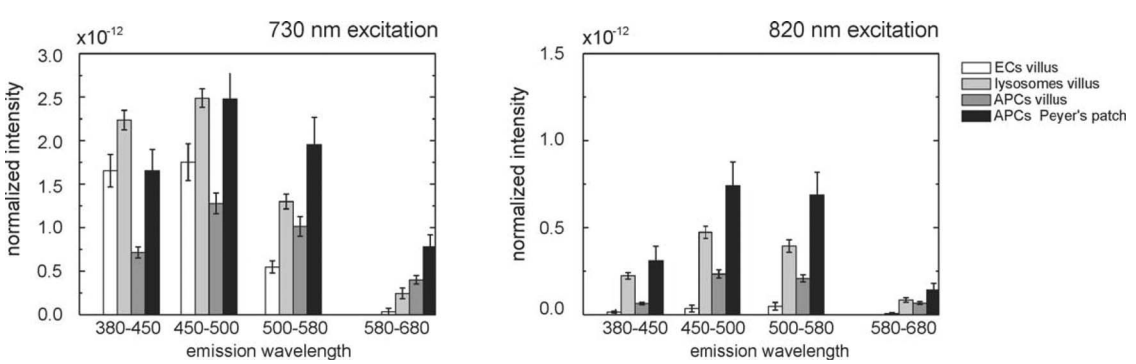

Fig. 10 Emission spectra of epithelial cells (ECs), lysosomes and APCs at 730- and 820-nm excitation.

Table 1 Ratiometric comparison of autofluorescence emission for cytoplasm of enterocytes (ECs), lysosomes and antigen presenting cells (APCs) in an intestinal villus and antigen presenting cells in a Peyer's patch. Ratios of the normalized intensity values in the four spectral emission channels (ch1–ch 4) were calculated for the data of Fig. 7.

(a) Ratio of fluorescence emission intensities at 730-nm excitation wavelength

	ch2/ch1	ch2/ch3	ch2/ch4
Villus ECs	1.06 ± 0.18	3.20 ± 0.56	51.1 ± 57
Villus lysosomes	1.11 ± 0.07	1.91 ± 0.15	10.2 ± 2.6
Villus APCs	1.79 ± 0.23	1.26 ± 0.18	3.19 ± 0.49
Peyer's patch APCs	1.50 ± 0.29	1.27 ± 0.26	3.18 ± 0.69

(b) Ratio of fluorescence emission intensities at 820-nm excitation wavelength

	ch1/ch2	ch1/ch3	ch1/ch4
Villus ECs	2.42 ± 1.6	0.73 ± 0.54	5.65 ± 5.7
Villus lysosomes	2.12 ± 0.24	1.20 ± 0.14	5.61 ± 0.94
Villus APCs	3.67 ± 0.53	1.12 ± 0.16	3.5 ± 0.53
Peyer's patch APCs	2.39 ± 0.78	1.08 ± 0.29	5.25 ± 1.71

(c) Ratio of fluorescence emission intensities at 730-nm and 820-nm excitation wavelengths.

	ch1(730 nm)/ ch1(820 nm)	ch2(730 nm)/ ch2(820 nm)	ch3(730 nm)/ ch3(820 nm)	ch4(730 nm)/ ch4(820 nm)
Villus ECs	114 ± 44	50 ± 29	11 ± 6	5.5 ± 7.6
Villus lysos.	10 ± 1.0	5.3 ± 0.5	3.3 ± 0.4	2.9 ± 0.8
Villus APCs	11 ± 1.5	5.5 ± 0.8	4.9 ± 0.7	6.0 ± 1.0
Peyer's patch APCs	5.4 ± 1.6	3.4 ± 0.7	2.8 ± 0.7	5.5 ± 1.8

excitation wavelength at 730 or 820 nm. The short-wavelength emission intensity at 730-nm compared to 820-nm excitation is twice as bright for macrophages in the lamina proria of the villi than for dendritic cells in the subepithelial dome area of Peyer's patches [ch1(730 nm)/ch1(820 nm)]. Likewise, the higher ratios of ch3(730 nm)/ch3(820 nm) and ch4(730 nm)/ch4(820 nm) for antigen-presenting cells in a villus points to a redshifted emission spectrum at 730-nm excitation as compared to lysosomes. This points to an additional autofluorescence component with larger Stokes shift in antigen-presenting cells.

3.3 *Correlation of Spectral Cell Signatures to Endogenous Fluorochromes*

In order to identify the fluorochromes contributing to the autofluorescence signal, the spatial distribution of the fluorescence and the recorded excitation-emission spectra are compared to the known morphology of the cells and literature data of endogeneous fluorescent chromophores contained in the studied tissue components [Figs. 2 and 8(b)]. The comparison indicates that autofluorescence in enterocytes arises mainly from NAD(P)H, which is abundant in high concentrations at the mitochondria and in lower concentrations in the cytosol. The regions of interest in the apical part of enterocytes comprise the cytosol and everything that is located within this selected part of the cell, for example mitochondria. In the normalized excitation spectra of the tissue components, the wavelength dependence of the two-photon action cross sections of the fluorescent chromophores is reflected in the slope of the spectra. The steep decrease of spectral amplitude with increasing wavelength observed for cytosol of enterocytes corresponds well with the literature data for NADH [solid line in Fig. 8(b)]. The value for the action cross section of NADH drops by one and a half orders of magnitude between 730 and 800 nm, and so does the normalized fluorescence intensity value that was measured for the apical cytoplasm of enterocytes. Figure 2(b) shows that the spectral emission of NAD(P)H is maximal around 470 nm and, thus, predominantly is detected in channels 2 and 1 with a small contribution in channel 3. This corresponds well to the spectral emission pattern measured for the cytoplasm of enterocytes. Though riboflavin or retinol have similar spectral characteristics, their low concentration in these cells and the distribution pattern of the fluorescence, which matches the distribution of the mitochondria, lead to the conclusion that NADH contributes mostly the the fluorescence of the enterocytes.

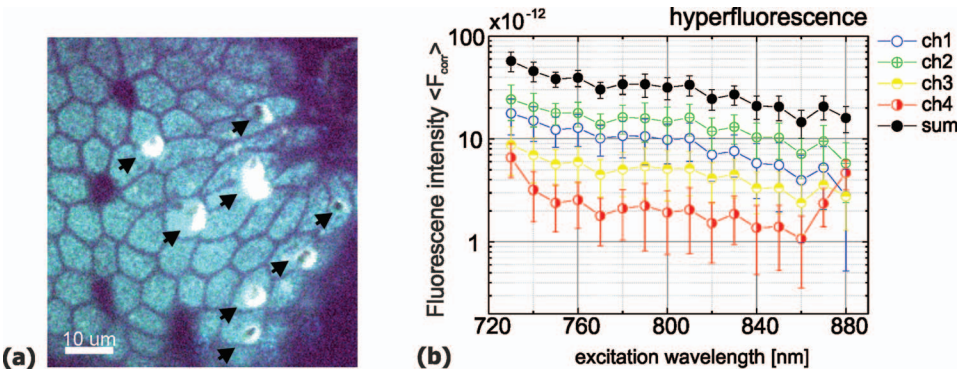

Fig. 11 Hyperfluorescence after repeated scanning irradiation. (a) Section of an autofluorescence image of an intestinal villus tip after it was scanned seven times with an average excitation power of 37.9 mW and excitation wavelength 730 nm. This is about 1.5 times more average power than what was usually used for autofluorescence imaging. Scan time per frame and field of view were 7.4 s and 150 × 150 μm^2. Hyperfluorescent regions are marked by arrowheads. (b) Excitation-emission spectrum of hyperfluorescent regions. The intensity increase in channel 4 at 730 and 870–880 nm is due to excitation stray light.

In lysosomes of enterocytes and in antigen-presenting cells that contain lysosomes, the fluorescence signal seems to have a high contribution from flavins and lipopigments. Lysosomal membranes contain FAD,[37] which emits around 550 nm [flavins, Fig. 2(b)] and can be efficiently excited over the whole tuning range of the laser [Fig. 8(b)]. The good visibility of the lysosomal signal over all excitation wavelengths [Figs. 6 and 8(a)] and the generally much higher fluorescence intensity of lysosomes and antigen-presenting cells compared to other tissue structures corresponds well with the high two-photon action cross section of FAD [Fig. 8(b)]. Another possible fluorescence source within lysosomes are lipopigments that accumulate within lysosomes as a result of degradation of lipids. The emission spectrum of lipopigments is very broad, with a maximum ~550 nm [Fig. 2(b)]. The lipopigment lipofuscin is found in granules of 1–5 μm size within the cytoplasm of metabolically active cells, such as the retinal pigment epithelium[38] and has been described also in enterocytes.[39] Lipofuscin has a high two-photon action cross section,[15] and its excitation maximum covers the broad range from 700 to 850 nm, which corresponds well to the excitation spectra of lysosomes measured in the present study (Figs. 9 and 10). The strong contribution of fluorescence emission from lysosomes in channel 3, where the FAD and lipopigment signal are measured, further corroborates the link of lysosomal autofluorescence to these chromophores. In addition, the bright punctuate regions in the apical cytoplasm of enterocytes in fixed sections of rat intestinal villi have been associated with storage of indoleamines, a group of neurotransmitters based on three-photon excited UV-emission of <400 nm.[15] We are unable to confirm this interpretation because our setup cannot detect fluorescence of <400 nm. However, it seems likely that lysosomes contain a mixture of the above-mentioned chromopores, including indoleamines.

3.4 *Rapid Fluorescence Increase and Photodamage*

Besides identifying tissue constituents, the spectral information allows one to also monitor changes of cell state induced by the laser irradiation. When the exposure due to scanning irradiation is too high, after a certain irradiance time, suddenly, a bright fluorescence associated with cell damage appears (Fig. 11). The fluorescence intensity increases to a level 10 and 40 times higher than the lysosome or cytosol fluorescence, respectively. Typically, the increase in fluorescence intensity, which we name hyperfluorescence, is first noted in channel 4, where the normal autofluorescence signal is very weak. Although hyperfluorescence during two-photon excited fluorescence microscopy has been observed previously,[40] the underlying damage mechanism remains unclear, and the hyperfluorescent substances have not yet been identified. We measured the characteristic spectral properties of the hyperfluorescence to provide additional information that may shed some light on this issue [Fig. 11(b)]. The fluorescence excitation spectrum exhibits a weak, monotonous decay with increasing wavelength. The emission spectrum shows, for all excitation wavelengths, a maximum in the green channel (450–500 nm) and is quite strong also in the blue channel (400–450 nm). The contribution in the red emission channel (600–680 nm) is weaker than in the other channels but is much stronger for hyperfluorescent regions than for cells that are not yet photodamaged. The wavelength dependence of the total hyperfluorescence intensity (sum of all channels) resembles that of antigen presenting cells. However, the spectral emission of hyperfluorescence peaks at shorter wavlengths (channels 1 and 2) while it is maximal in channels 2 and 3 for antigen-presenting cells. This difference indicates a different chemical composition of the relevant fluorophores. Chemical changes of cellular substances may be induced directly by two- or three-photon processes[41] but also indirectly via free-electron generation that results in chemical bond breaking.[42] The sudden onset of hyperfluorescence is indicative for a "runaway process" governing the generation of the fluorescent substances once a threshold is overcome. In our experiments, hyperfluorescence commenced at roughly two times the average excitation power that was normally used for imaging at 730 nm (20 mW instead of 12 mW, data not shown). The fact that hyperfluorescence starts only after a certain irradiance time suggests that dose-dependent photochemical processes are involved. These processes may form new highly fluorescing absorbers. If the newly formed absorbers contribute themselves to the photochemical process then a hyperfluorescence "runaway" starts once a certain threshold concentration is exceeded.

This mechanism would explain the observed sudden buildup and rapid enlargement of the hyperfluorescent areas.

4 Conclusions

We demonstrated spectrally resolved time-lapse two-photon imaging of cellular dynamics in murine small intestine in three dimensions over up to 8 h. We showed that imaging based solely on autofluorescence provides good intrinsic contrast between different cell types, cell organelles, and other tissue components of the intestine. We investigated the autofluorescence intensity spectra of different cell types and cell organelles and found marked differences between enterocytes, antigen-presenting cells, and lysosomes. As concluded by the excitation spectra, autofluorescence of all named tissue components is excited simultaneously at a 730-nm excitation wavelength, while an excitation wavelength of >820 nm is best suited to selectively excite antigen-presenting cells and lysosomes within enterocytes and to induce SHG at the collagen scaffold of the extracellular matrix. We related the spectral signatures of cell types and cell organelles to the spectra of endogenous fluorophores and concluded that autofluorescence in the cytoplasm of enterocytes is mainly due to NAD(P)H. We identified the bright punctuate cell organelles in the apical cytoplasm of enterocytes and within antigen-presenting cells as lysosomes that contain FAD and lipopigments.

Strong and long-lasting irradiation of the mucosal tissue induced hyperfluorescence associated with cell damage. The excitation-emission spectra of the hyperfluorescence indicate that it arises from a chemical substance with either the high concentration or high two-photon absorption cross section that was absent before laser irradiation. The sudden onset of hyperfluorescence suggests that the chemical composition of the tissue is modified locally in a nonlinear process when both a certain irradiation dose and a certain irradiance threshold are exceeded. In our experiments, this occured when the power exceeded a value roughly two times higher than the average excitation power that was normally used for autofluorescence imaging at 730 nm.

In the future, automated segmentation based on autofluorescence fingerprints may be implemented to follow individual cells over long time periods. This feature would facilitate investigations of cell–cell interaction occuring during immunologic processes at this important mucosal interface. In order to selectively follow antigen-presenting cells, the use of two different laser wavelengths, for example, 730 and 820 nm, is best suited to discriminate antigen-presenting cells and surrounding tissue. However, because the cells are rapidly moving and acquisition of one image takes $\sim$10 s, a sequential imaging with two different excitation wavelengths is not fast enough to capture the same tissue state. Therefore, interlaced excitation with two different wavelengths is desirable in order to be able to superimpose the images. With such a setup, a ratiometric comparison of fluorescence intensities in the different emission channels could be used for an online discrimination of different cells or cell organelles. Moreover, in order to tackle immunological questions, further discrimination of cellular subtypes of antigen-presenting cells, such as dendritic cells, B, and T lymphocytes is needed that may require the combination of exogenous markers with the autofluorescence-based spectral fingerprinting explored in this study.

Acknowledgments

We thank Norbert Koop for excellent technical assistance. This work was supported by the German research foundation (DFG), Projects No. Hu 629/3-1 and No. Ge 647/9-1.

References

1. A. Didierlaurent, J.-C. Sirard, J.-P. Kraehenbuhl, and M. R. Neutra, "How the gut senses its content," *Cell. Microbiol.* **4**(2), 61–72 (2002).
2. A. Gebert, "The role of M cells in the protection of mucosal membranes," *Histochem. Cell Biol.* **108**(6), 455–470 (1997).
3. P. Brandtzaeg, E. S. Baekkevold, I. N. Farstad, F. L. Jahnsen, F.-E. Johansen, E. M. Nilsen, and T. Yamanaka, "Regional specialization in the mucosal immune system: what happens in the microcompartments?" *Immunol. Today* **20**(3), 141–151 (1999).
4. J. Büning, G. Hundorfean, M. Schmitz, K.-P. Zimmer, S. Strobel, A. Gebert, and D. Ludwig, "Antigen targeting to MHC class II-enriched late endosomes in colonic epithelial cells: trafficking of luminal antigens studied *in vivo* in Crohn's colitis patients," *FASEB J.* **20**(2), 359–61 (2006).
5. W. Denk, J. H. Strickler, and W. W. Webb, "Two-photon laser scanning fluorescence microscopy," *Science* **248**, 73–76 (April 1990).
6. C. Xu and W. W. Webb, "Measurement of two-photon excitation cross sections of molecular fluorophores with data from 690 to 1050 nm," *J. Opt. Soc. Am. B* **13**(3), 481–491 (1996).
7. F. Helmchen and W. Denk, "Deep tissue two-photon microscopy," *Nat. Meth.* **2**(12), 932–940 (2005).
8. B. H. Zinselmeyer, J. N. Lynch, X. Zhang, T. Aoshi, and M. J. Miller, "Video-rate two-photon imaging of mouse footpad - a promising model for studying leukocyte recruitment dynamics during inflammation," *Inflamm. Res.* **57**(3), 93–96 (2008).
9. K. W. Dunn, R. M. Sandoval, K. J. Kelly, P. C. Dagher, G. A. Tanner, S. J. Atkinson, R. L. Bacallao, and B. A. Molitoris, "Functional studies of the kidney of living animals using multicolor two-photon microscopy," *Am. J. Physiol. Cell Physiol.* **283**, C905–C916 (2002).
10. T. Mempel, S. Henrickson, and U. Von Andrian, "T-cell priming by dendritic cells in lymph nodes occurs in three distinct phases," *Nature* **427**(6970), 154–159 (2004).
11. V. Konjufca and M. J. Miller, "Two-photon microscopy of host-pathogen interactions: acquiring a dynamic picture of infection *in vivo*," *Cell. Microbiol.* **11**(4), 551–559 (2009).
12. A. J. M. Watson, S. Chu, L. Sieck, O. Gerasimenko, T. Bullen, F. Campbell, M. McKenna, T. Rose, and M. H. Montrose, "Epithelial barrier function *in vivo* is sustained despite gaps in epithelial layers," *Gastroenterology* **129**(3), 902–912 (2005).
13. M. Chieppa, M. Rescigno, A. Y. C. Huang, and R. N. Germain, "Dynamic imaging of dendritic cell extension into the small bowel lumen in response to epithelial cell TLR engagement," *J. Exp. Med.* **203**(13), 2841–2852 (2006).
14. H. Bao, A. Boussioutas, J. Reynolds, S. Russell, and M. Gu, "Imaging of goblet cells as a marker for intestinal metaplasia of the stomach by one-photon and two-photon fluorescence endomicroscopy," *J. Biomed. Opt.* **14**(6), 064031 (2010).
15. W. R. Zipfel, R. M. Williams, R. Christie, A. Y. Nikitin, B. T. Hyman, and W. W. Webb, "Live tissue intrinsic emission microscopy using multiphoton-excited native fluorescence and second harmonic generation," *Proc. Natl. Acad. Sci. U S A* **100**(12), 7075–7080 (2003).
16. P. J. Campagnola, A. C. Millard, M. Terasaki, P. E. Hoppe, C. J. Malone, and W. A. Mohler, "Three-dimensional high-resolution second-harmonic generation imaging of endogenous structural proteins in biological tissues," *Biophys. J.* **81**, 493–508 (2002).
17. A. Zoumi, A. Yeh, and B. J. Tromberg, "Imaging cells and extracellular matrix *in vivo* by using second-harmonic generation and two-photon excited fluorescence," *Proc. Natl. Acad. Sci. U S A* **99**(17), 11014–11019 (2002).
18. P. Steven, J. Rupp, G. Hüttmann, N. Koop, C. Lensing, H. Laqua, and A. Gebert, "Experimental induction and three-dimensional two-photon imaging of conjunctiva-associated lymphoid tissue," *Invest. Ophthalmol. Vis. Sci.* **49**, 1512–1517 (2008).
19. J. M. Crawford and N. S. Braunwald, "Toxicity in vital fluorescence microscopy: effect of dimethylsulfoxide, rhodamine-123, and Dil-Low

density lipoprotein on fibroblast growth *in vitro*," *in Vitro Cell. & Dev. Biol.* **27A**(8), 633–638 (1991).
20. J. A. Palero, H. S. de Bruijn, A. van der Ploeg van den Heuvel, H. J. C. M. Sterenborg, and H. C. Gerritsen, "Spectrally resolved multiphoton imaging of *in vivo* and excised mouse skin tissues," *Biophys. J.* **93**, 992–1007 (2007).
21. J. V. Rocheleau, W. S. Head, and D. W. Piston, "Quantitative NAD(P)H/flavoprotein autofluorescence imaging reveals metabolic mechanisms of pancreatic islet pyruvate response," *J. Biol. Chem.* **279**(30), 31780–31787 (2004).
22. J. A. Palero, A. N. Bader, H. S. de Bruijn, A. van der Ploeg van den Heuvel, H. J. C. M. Sterenborg, and H. C. Gerritsen, "*in vivo* monitoring of protein-bound and free NADH during ischemia by nonlinear spectral imaging microscopy," *Biomed. Opt. Express.* **2**(5), 1030–1039 (2011).
23. A. J. Radosevich, M. B. Bouchard, S. A. Burgess, B. R. Chen, E. M. Hillman, "Hyperspectral *in vivo* two-photon microscopy of intrinsic contrast," *Opt. Lett.* **33**, 2164–2166 (2008).
24. J. Chen, A. Lee, J. Zhao, H. Wang, H. Lui, D. I. McLean, H. Zeng, "Spectroscopic characterization and microscopic imaging of extracted and in situ cutaneous collagen and elastic tissue components under two-photon excitation," *Skin Res.Technol.* **15**(4), 418–426 (2009).
25. S. Huang, A. A. Heikal, and W. W. Webb, "Two-photon fluorescence spectroscopy and microscopy of NAD(P)H and flavoprotein," *Biophys. J.* **78**, 2811–2825 (2002).
26. D.-W. Piston and S. M. Knobel, "Quantitative imaging of metabolism by two-photon excitation microscopy," *Methods Enzymol.* **307**, 351–368 (1999).
27. G. A. Wagnières, W. M. Star, and B. C. Wilson, "*In vivo* fluorescence spectroscopy and imaging for oncological applications," *Photochem. Photobiol.* **68**, 603–632 (1998).
28. Y. Mochizuki, M. K. Park, T. Mori, and S. Kawashima, "*The difference in autofluorescence features of lipofuscin between brain and adrenal*," *Zool. Sci.*, **12**(3), pp. 283–288 (1995).
29. Image-analysis Software ImageJ, <http://rsbweb.nih.gov/ij>.
30. Q. Zhang, D. W. Piston, and R. H. Goodman, "Regulation of corepressor function by nuclear NADH," *Science* **295**, 1895–1897 (2002).
31. D. A. Hume, V. H. Perry, and S. Gordon, "The mononuclear phagocyte system of the mouse defined by immunohistochemical localisation of antigen F4/80: macrophages associated with epithelia," *Anat. Rec.* **210**(3), 503–512 (1984).
32. L. Mayer, A. Panja, Y. Li, E. Siden, A. Pizzimenti, F. Gerardi, and N. Chandswang, "Unique features of antigen presentation in the intestine," *Ann. NY Acad. Sci* **664**, 39–46 (1992).
33. T. L. Denning, Y.-c. Wang, S. R. Patel, I. R. Williams, and B. Pulendran, "Lamina propria macrophages and dendritic cells differentially induce regulatory and interleukin 17-producing T cell responses." *Nat. Immunol.* **8**(10), 1086–1094 (2007).
34. L. E. Smythies, M. Sellers, R. H. Clements, M. Mosteller-Barnum, G. Meng, W. H. Benjamin, J. M. Orenstein, and P. D. Smith, "Human intestinal macrophages display profound inflammatory anergy despite avid phagocytic and bacteriocidal activity," *J. Clin. Invest.* **115**(1), 66–75 (2005).
35. B. L. Kelsall and W. Strober, "Distinct populations of dendritic cells are present in the subepithelial dome and T cell regions of the murine Peyer's patch," *J. Exp. Med.* **183**(1), 237–247 (1996).
36. M. Neutra, "Current concepts in mucosal immunity. V. role of M cells in transepithelial transport of antigens and pathogens to the mucosal immune system," *Am J Physiol.* **274**, G785–791 (1998).
37. H.-J. Shin and J.-L. Mego, "A rat liver lysosomal membrane flavin-adenine dinucleotide phosphohydrolase: purification and characterization," *Arch. Biochem. Biophys.* **267**, 95–103 (1988).
38. R. Richards-Kortum and E. Sevick-Muraca, Quantitative optical spectroscopy for tissue diagnosis, *Annu. Rev. Phys. Chem.* **47**, 555606 (1996).
39. R. T. Bronson, "Ultrastructure of Macrophages and Karyolytic Bodies in Small Intestinal Villi of Macaque Monkeys and Baboons," *Vet. Pathol.* **18**(6), 727–737 (1981).
40. L. M. Tiede and M. G. Nichols, "Photobleaching of reduced nicotinamide andenine dinucleotide and the development of highly fluorescent lesions in rat basophilic leukemia cells during multiphoton microscopy," *Photochem. Photobiol.* **82**, 656–664 (2006).
41. D. N. Nikogosyan, "Two-quantum UV photochemistry of nucleic acids: comparison with conventional low-intensity UV photochemistry and radiation chemistry." *Int. J. Radiat. Biol.* **57**(2), 233–99 (1990).
42. A. Vogel, J. Noack, G. Hüttman, G. Paltauf, "Mechanisms of femtosecond laser nanosurgery of cells and tissues," *Appl. Phys. B - Lasers O.* **81**(8), 1015–1047 (2005).